

Differential Dynamic Programming Neural Optimizer

Guan-Horng Liu, Tianrong Chen, and Evangelos A. Theodorou
 Autonomous Control and Decision Systems Laboratory
 Georgia Institute of Technology, Atlanta, GA 30332
 {ghliu, tianrong.chen, evangelos.theodorou}@gatech.edu

Abstract

Interpretation of Deep Neural Networks (DNNs) training as an optimal control problem with nonlinear dynamical systems has received considerable attention recently, yet the algorithmic development remains relatively limited. In this work, we make an attempt along this line by reformulating the training procedure from the trajectory optimization perspective. We first show that most widely-used algorithms for training DNNs can be linked to the Differential Dynamic Programming (DDP), a celebrated second-order trajectory optimization algorithm rooted in the Approximate Dynamic Programming. In this vein, we propose a new variant of DDP that accepts batch optimization for training feedforward networks, while integrating naturally with the curvature approximation in existing methods. The resulting algorithm features layer-wise feedback policies which improve convergence and reduce sensitivity to hyper-parameter over existing methods. We show that the algorithm is competitive against state-of-the-art first and second order methods, and have surprising benefit in preventing gradient vanishing. Our work opens up new avenues for principled algorithmic design built upon the optimal control theory.

1 Introduction

In this work, we consider the following optimal control problem (OCP) in the discrete-time setting:

$$\min_{\bar{\mathbf{u}}} J(\bar{\mathbf{u}}; \mathbf{x}_0) := \left[\phi(\mathbf{x}_T) + \sum_{t=0}^{T-1} \ell_t(\mathbf{x}_t, \mathbf{u}_t) \right] \quad \text{s.t. } \mathbf{x}_{t+1} = f_t(\mathbf{x}_t, \mathbf{u}_t), \quad (\text{OCP})$$

where $\mathbf{x}_t \in \mathbb{R}^n$ and $\mathbf{u}_t \in \mathbb{R}^m$ represent the state and control at each time step t . $f_t(\cdot, \cdot)$, $\ell_t(\cdot, \cdot)$ and $\phi(\cdot)$ respectively denote the nonlinear dynamics, intermediate cost and terminal cost functions. OCP aims to find a control trajectory, $\bar{\mathbf{u}} \triangleq \{\mathbf{u}_t\}_{t=0}^{T-1}$, such that the accumulated cost J over the finite horizon $t \in \{0, 1, \dots, T\}$ is minimized. Problems with the form of OCP appear in multidisciplinary areas since it describes a generic multi-stage decision making problem, and have gained commensurate interest recently in deep learning.

Central to the research along this line is the interpretation of DNNs as discrete-time nonlinear dynamical systems, in which each layer is viewed as a distinct time step [1]. The dynamical system perspective provides sound explanation for the success of certain DNN architectures [2]. It also enables principled architecture design by bringing rich analysis from numerical differential equations [3, 4] and discrete mechanism [5, 6] when learning problems inherit physical structures. In the continuum limit of depth, Chen et al. [7] parametrized an ordinary differential equation (ODE) directly using DNNs, later with Liu et al. [8] extending the framework to accept stochastic dynamics.

From the optimization viewpoint, when the network weight is recast as the control variable, OCP describes without loss of generality the training objective composed of layer-wise loss (e.g. weight

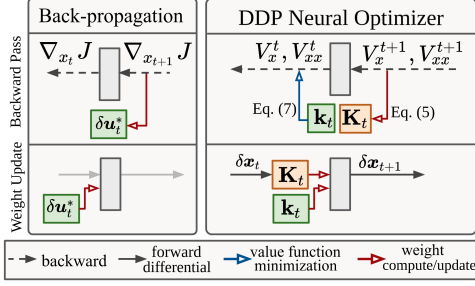


Table 1: Terminology mapping

	Deep Learning	Optimal Control
J	Total Loss	Trajectory Cost
\mathbf{x}_t	Activation Vector	State Vector
\mathbf{u}_t	Weight Parameter	Control Vector
f	Layer Propagation	Dynamical System
ϕ	End-goal Loss	Terminal Cost
ℓ	Weight Decay	Intermediate Cost

Figure 1: (Right) Computational graphs in the backward pass (upper) and weight update (lower). DDP differs from Back-propagation in that (1) the value derivatives $V_{\mathbf{x}}, V_{\mathbf{x}\mathbf{x}}$, as opposed to the loss gradient $\nabla_{\mathbf{x}} J$, are computed backward, and (2) the weight parameter is updated using layer-wise feedback policies, denoted \mathbf{k}_t and \mathbf{K}_t , with additional forward propagation.

decay) and terminal loss (e.g. cross-entropy). This connection has been mathematically explored in many recent works [9, 10, 11]. Despite they provide theoretical statements for convergence and generalization, the algorithmic development remains relatively limited. Specifically, previous works primarily focus on applying first-order optimality conditions, provided by the Pontryagin principle [12], to architectures restricted to residual blocks or discrete weights [13, 14, 15].

In this work, we take a parallel path from the Approximate Dynamic Programming [16] (ADP), a technique particularly designed to solve complex Markovian decision processes. For this kind of problems, ADP has been shown numerically superior to *direct* optimization such as Newton method since it takes into account the temporal structure inherit in OCP [17]. The resulting update law features a locally optimal feedback policy at each stage (see Fig. 1), which is in contrast to the one derived from the Pontryagin’s principle. In the application of DNNs, we will show through experiments that these policies help improve training convergence and robustness to hyper-parameters.

Of our particular interest among practical ADP algorithms is the Differential Dynamic Programming (DDP) [18]. DDP is a second order method that has been used extensively for complex trajectory optimization in robotics [19, 20]. In this work we further show that existing first and second order methods for training DNNs can be derived from DDP as special cases (see Table 2). Such an intriguing connection can be beneficial to both sides. While we can leverage recent advances in efficient curvature factorization of the loss Hessian [21, 22] to relieve the computational burden in DDP, on the other hand, computing feedback policies stands as an independent module; thus it can be integrated into existing first and second order methods.

The concept of feedback mechanism has already shown up in the study of network design, where the terminology typically refers to connections between modules over training [23, 24] or successive prediction for vision applications [25, 26]. Conceptually perhaps Shama et al. [27], Huh et al. [28] are most related to our work, where the authors proposed to reuse the discriminator from a Generative Adversarial Network as a feedback module during training or test time. We note that, however, neither the problem formulation nor the mapping space of the feedback module is the same as ours. Our feedback policy is originated from the optimal control theory in which control update needs to compensate the state disturbance throughout propagation.

The paper is organized as follows. In Sec. 2 we go over optimality conditions to OCP and review the DDP algorithm. Connection between DNNs training and trajectory optimization is solidified in Sec. 3, with a practical algorithm demonstrated in Sec. 4. We provide empirical results in Sec. 5.

2 Preliminaries

Optimality Conditions to OCP: Development of the optimality conditions to OCP can be dated back to 1960s, characterized by the Pontryagin’s Maximum Principle (PMP) and the Dynamic Programming (DP). We detail the two different approaches below.

Notation: We will always use t as the time step of dynamics and denote a trajectory as $\bar{\mathbf{x}} \triangleq \{\mathbf{x}_t\}_{t=0}^{T-1}$. Given a time-dependent functional $\mathcal{F}_t(\mathbf{x}_t, \mathbf{u}_t) : \mathbb{X} \times \mathbb{U} \mapsto \mathbb{R}$, we will denote and abbreviate its Jacobian and Hessian respectively as $\nabla_{\mathbf{x}} \mathcal{F}_t \equiv \mathcal{F}_{\mathbf{x}}^t$ and $\nabla_{\mathbf{x}\mathbf{x}} \mathcal{F}_t \equiv \mathcal{F}_{\mathbf{x}\mathbf{x}}^t$.

Theorem 1 (Discrete-time PMP [29]). *Let $\bar{\mathbf{u}}^*$ be the optimal control trajectory for OCP and $\bar{\mathbf{x}}^*$ be the corresponding state trajectory. Then, there exists a co-state trajectory $\bar{\mathbf{p}}^* \triangleq \{\mathbf{p}_t^*\}_{t=1}^T$, such that*

$$\mathbf{x}_{t+1}^* = \nabla_{\mathbf{p}} H_t(\mathbf{x}_t^*, \mathbf{p}_{t+1}^*, \mathbf{u}_t^*), \quad \mathbf{x}_0^* = \mathbf{x}_0, \quad (1)$$

$$\mathbf{p}_t^* = \nabla_{\mathbf{x}} H_t(\mathbf{x}_t^*, \mathbf{p}_{t+1}^*, \mathbf{u}_t^*), \quad \mathbf{p}_T^* = \nabla_{\mathbf{x}} \phi(\mathbf{x}_T^*), \quad (2)$$

$$\mathbf{u}_t^* = \arg \min_{\mathbf{v} \in \mathbb{R}^m} H_t(\mathbf{x}_t^*, \mathbf{p}_{t+1}^*, \mathbf{v}). \quad (3)$$

where $H_t : \mathbb{R}^n \times \mathbb{R}^n \times \mathbb{R}^m \mapsto \mathbb{R}$ is the discrete-time Hamiltonian given by $H_t(\mathbf{x}_t, \mathbf{p}_{t+1}, \mathbf{u}_t) \triangleq \ell_t(\mathbf{x}_t, \mathbf{u}_t) + \mathbf{p}_{t+1}^\top f_t(\mathbf{x}_t, \mathbf{u}_t)$, and Eq. (2) is called adjoint equation.

The discrete-time PMP theorem can be derived using KKT conditions, in which the co-state \mathbf{p}_t is equivalent to the Lagrange multiplier. As we will see in section 3.1, the adjoint dynamics Eq. (2) has a direct link to the Back-propagation. Note that the solution to Eq. (3) admits an open-loop process in the sense that it does not depend on state variables. This is in contrast to the Dynamic Programming (DP) principle, in which a feedback policy is considered.

Theorem 2 (DP [30]). *Define a value function $V_t : \mathbb{R}^n \mapsto \mathbb{R}$ at each time step that is computed backward in time using the Bellman equation*

$$V_t(\mathbf{x}_t) = \min_{\mathbf{u}_t \in \Gamma_{\mathbf{x}_t}} \underbrace{\ell_t(\mathbf{x}_t, \mathbf{u}_t) + V_{t+1}(f_t(\mathbf{x}_t, \mathbf{u}_t))}_{\triangleq Q_t(\mathbf{x}_t, \mathbf{u}_t)}, \quad V_T(\mathbf{x}_T) = \phi(\mathbf{x}_T), \quad (4)$$

where $\Gamma_{\mathbf{x}_t} : \mathbb{R}^n \mapsto \mathbb{R}^m$ denotes a set of mapping from state to control space. Then, we have $V_0(\mathbf{x}_0) = J^*(\mathbf{x}_0)$ be the optimal objective value to OCP. Furthermore, if $\mathbf{u}_t^* = \mu_t^*(\mathbf{x}_t)$ minimizes the RHS of Eq. (4), then the policy $\pi^* = \{\mu_0^*, \dots, \mu_{T-1}^*\}$ is optimal.

Hereafter we refer $Q_t(\mathbf{x}_t, \mathbf{u}_t)$ to the *Bellman objective*. The principle of DP recasts the problem of minimizing over a control sequence to a sequence of minimization over each control. The value function V_t summarizes the optimal cost-to-go at each stage, provided all afterward stages also being minimized. π^* is an optimal policy in a globally convergent closed loop system.

Differential Dynamic Programming (DDP): Trajectory optimization algorithms typically solve the optimality equations from PMP or DP. Unfortunately, solving Eq. (4) in high-dimensional problems appears infeasible, well-known as the Bellman curse of dimensionality. To mitigate the computational burden from the minimization involved at each stage, one can replace the Bellman objective in Eq. (4) with its second order Taylor expansion. Such an approximation is central to DDP, a second-order method that inherits a similar Bellman optimality structure while being computationally efficient.

Alg. 1 summarizes the DDP algorithm. Given a nominal trajectory $(\bar{\mathbf{x}}, \bar{\mathbf{u}})$, DDP iteratively optimizes its accumulated cost, where each iteration consists a backward (lines 2-6 in Alg. 1) and forward pass (lines 7-11 in Alg. 1). During the backward pass, DDP expands the Bellman objective at each stage up to second-order, i.e. $Q_t(\mathbf{x}_t + \delta \mathbf{x}_t, \mathbf{u}_t + \delta \mathbf{u}_t) \approx Q_t(\mathbf{x}_t, \mathbf{u}_t) + \delta Q_t(\delta \mathbf{x}_t, \delta \mathbf{u}_t)$, where

$$\delta Q_t = \frac{1}{2} \begin{bmatrix} \mathbf{1} \\ \delta \mathbf{x}_t \\ \delta \mathbf{u}_t \end{bmatrix}^\top \begin{bmatrix} \mathbf{0} & Q_x^t & Q_u^t \\ Q_x^t & Q_{xx}^t & Q_{xu}^t \\ Q_u^t & Q_{ux}^t & Q_{uu}^t \end{bmatrix} \begin{bmatrix} \mathbf{1} \\ \delta \mathbf{x}_t \\ \delta \mathbf{u}_t \end{bmatrix}, \quad \begin{aligned} Q_x^t &= \ell_x^t + f_x^{t\top} V_x^{t+1} \\ Q_u^t &= \ell_u^t + f_u^{t\top} V_x^{t+1} \\ Q_{xx}^t &= \ell_{xx}^t + f_x^{t\top} V_{xx}^{t+1} f_x^t + V_x^{t+1} \cdot f_{xx}^t \\ Q_{uu}^t &= \ell_{uu}^t + f_u^{t\top} V_{xx}^{t+1} f_u^t + V_x^{t+1} \cdot f_{uu}^t \\ Q_{ux}^t &= \ell_{ux}^t + f_u^{t\top} V_{xx}^{t+1} f_x^t + V_x^{t+1} \cdot f_{ux}^t \end{aligned} \quad (5)$$

The derivatives of Q_t follow standard chain rule and the dot notation represents the product of a vector with a 3D tensor. The optimal policy in this case admits a linear form given by

$$\delta \mathbf{u}_t^*(\delta \mathbf{x}_t) = \mathbf{k}_t + \mathbf{K}_t \delta \mathbf{x}_t = -(Q_{uu}^t)^{-1} (Q_u^t + Q_{ux}^t \delta \mathbf{x}_t), \quad (6)$$

where $\delta \mathbf{x}_t$ is the state differential. \mathbf{k}_t and \mathbf{K}_t respectively denote the open and feedback gains. Note that this policy is only optimal *locally* around the nominal trajectory where the second order approximation remains valid. Substitute $\delta \mathbf{u}_t^*$ in Eq. (6) back to (5) will give us the backward update of the derivatives of value function:

$$V_x^t = Q_x^t - Q_{ux}^t (Q_{uu}^t)^{-1} Q_u^t, \quad \text{and} \quad V_{xx}^t = Q_{xx}^t - Q_{ux}^t (Q_{uu}^t)^{-1} Q_{ux}^t. \quad (7)$$

In the forward pass, DDP applies the feedback policy sequentially from the initial time step while keeping track of the state differential between the new simulated trajectory and the nominal trajectory.

Algorithm 1 Differential Dynamic Programming

```

1: Input:  $\bar{\mathbf{u}} \triangleq \{\mathbf{u}_t\}_{t=0}^{T-1}$ ,  $\bar{\mathbf{x}} \triangleq \{\mathbf{x}_t\}_{t=0}^T$ 
2: Set  $V_{\mathbf{x}}^T = \nabla_{\mathbf{x}} \phi$  and  $V_{\mathbf{x}\mathbf{x}}^T = \nabla_{\mathbf{x}\mathbf{x}} \phi$ 
3: for  $t = T - 1$  to 0 do
4:   Compute  $Q_{\mathbf{x}}^t, Q_{\mathbf{u}}^t, Q_{\mathbf{x}\mathbf{x}}^t, Q_{\mathbf{u}\mathbf{x}}^t, Q_{\mathbf{u}\mathbf{u}}^t$  with
     Eq. (5)
5:   Compute  $\mathbf{k}_t, \mathbf{K}_t, V_{\mathbf{x}}^t, V_{\mathbf{x}\mathbf{x}}^t$  with Eq. (6)-(7)
6: end for
7: Set  $\mathbf{x}_0^* = \mathbf{x}_0$ 
8: for  $t = 0$  to  $T - 1$  do
9:    $\mathbf{u}_t^* = \mathbf{u}_t + \mathbf{k}_t + \mathbf{K}_t \delta \mathbf{x}_t$ , ( $\delta \mathbf{x}_t = \mathbf{x}_t^* - \mathbf{x}_t$ )
10:   $\mathbf{x}_{t+1}^* = f_t(\mathbf{x}_t^*, \mathbf{u}_t^*)$ 
11: end for
12:  $\bar{\mathbf{u}} \leftarrow \bar{\mathbf{u}}^*$ 

```

Algorithm 2 Back-propagation with Gradient Descent

```

1: Input:  $\bar{\mathbf{u}} \triangleq \{\mathbf{u}_t\}_{t=0}^{T-1}$ ,  $\bar{\mathbf{x}} \triangleq \{\mathbf{x}_t\}_{t=0}^T$ , learning rate  $\eta$ 
2: Set  $\mathbf{p}_T = \nabla_{\mathbf{x}} \phi$ 
3: for  $t = T - 1$  to 0 do
4:    $\delta \mathbf{u}_t = \nabla_{\mathbf{u}_t} H_t = \nabla_{\mathbf{u}_t} \{\sigma_t(g_t(\mathbf{x}_t, \mathbf{u}_t))\}^\top \mathbf{p}_{t+1}$ 
5:    $\mathbf{p}_t = \nabla_{\mathbf{x}_t} H_t = \nabla_{\mathbf{x}_t} \{\sigma_t(g_t(\mathbf{x}_t, \mathbf{u}_t))\}^\top \mathbf{p}_{t+1}$ 
6: end for
7: for  $t = 0$  to  $T - 1$  do
8:    $\mathbf{u}_t^* = \mathbf{u}_t - \eta \delta \mathbf{u}_t$ 
9: end for
10:  $\bar{\mathbf{u}} \leftarrow \bar{\mathbf{u}}^*$ 

```

3 Training DNNs as Trajectory Optimization

3.1 Optimal Control Formulation

Recall that DNNs can be interpreted as dynamical systems in which each layer is viewed as a distinct time step. Consider for instance the mapping in feedforward networks,

$$\mathbf{x}_{t+1} = \sigma_t(\mathbf{h}_t), \quad \mathbf{h}_t = g_t(\mathbf{x}_t, \mathbf{u}_t) \equiv \mathbf{W}_t \mathbf{x}_t + \mathbf{b}_t. \quad (8)$$

$\mathbf{x}_t \in \mathbb{R}^{n_t}$ and $\mathbf{x}_{t+1} \in \mathbb{R}^{n_{t+1}}$ represent the activation vector at layer t and $t + 1$, with $\mathbf{h}_t \in \mathbb{R}^{n_{t+1}}$ being the pre-activation vector. σ_t and g_t respectively denote the nonlinear activation function and the affine transform parametrized by the weight $\mathbf{u}_t \triangleq [\text{vec}(\mathbf{W}_t), \mathbf{b}_t]^\top$. Eq. (8) can be seen as a dynamical system propagating the activation vector \mathbf{x}_t using \mathbf{u}_t .

It is natural to ask whether the necessary condition in the PMP theorem relates to first-order optimization methods in DNN training. This is indeed the case as pointed out in Li et al. [15]:

Lemma 3 ([15]). *Back-propagation satisfies Eq. (2) and gradient descent iteratively solves Eq. (3).*

Lemma 3 follows by first expanding the derivative of Hamiltonian wrt \mathbf{x}_t ,

$$\nabla_{\mathbf{x}_t} H_t(\mathbf{x}_t, \mathbf{p}_{t+1}, \mathbf{u}_t) = \nabla_{\mathbf{x}_t} \ell_t(\mathbf{x}_t, \mathbf{u}_t) + \nabla_{\mathbf{x}_t} f_t(\mathbf{x}_t, \mathbf{u}_t)^\top \mathbf{p}_{t+1} = \nabla_{\mathbf{x}_t} J(\bar{\mathbf{u}}; \mathbf{x}_0). \quad (9)$$

Thus, Eq. (2) is simply the chain rule used in the Back-propagation. When H_t is differentiable wrt \mathbf{u}_t , one can attempt to solve Eq. (3) by iteratively taking the gradient descent. This will lead to

$$\mathbf{u}_t^{(k+1)} = \mathbf{u}_t^{(k)} - \eta \nabla_{\mathbf{u}_t} H_t(\mathbf{x}_t, \mathbf{p}_{t+1}, \mathbf{u}_t) = \mathbf{u}_t^{(k)} - \eta \nabla_{\mathbf{u}_t} J(\bar{\mathbf{u}}; \mathbf{x}_0), \quad (10)$$

where k and η denote the update iteration and step size. Thus, existing optimization methods can be interpreted as iterative processes to match the PMP optimality conditions.

We now extend Lemma 3 to accept the batch setting. The following proposition will become useful as we proceed to the algorithmic design in the next section.

Proposition 4. (Informal; see Appendix A for full version) *Consider the batch samples $\{\mathbf{x}_t^{(i)}\}_{i=1}^B$ with the batch size B . Define $\mathbf{X}_t \triangleq [\cdots, \mathbf{x}_t^{(i)}, \cdots]^\top$ as the batch-augmented state with $\mathbf{J}(\bar{\mathbf{u}}; \mathbf{X}_0) \triangleq \frac{1}{B} \sum_B J(\bar{\mathbf{u}}; \mathbf{x}_0^{(i)})$ as the new objective. Then, iteratively solving the “augmented” PMP equations is equivalent to applying mini-batch gradient descent with Back-propagation. Specifically, the derivative of the batch-augmented Hamiltonian \mathbf{H}_t takes the exact form with the mini-batch gradient update:*

$$\nabla_{\mathbf{u}_t} \mathbf{H}_t(\mathbf{X}_t, \mathbf{P}_{t+1}, \mathbf{u}_t) = \frac{1}{B} \sum_i \nabla_{\mathbf{u}_t} J(\bar{\mathbf{u}}; \mathbf{x}_0^{(i)}), \quad \text{where } \mathbf{P}_{t+1} = \frac{1}{B} [\cdots, \mathbf{p}_{t+1}^{(i)}, \cdots]^\top. \quad (11)$$

Proposition 4 suggests that in the batch setting, we aim to find an ultimate open-loop control that can drive every data point in the sampled batch to its designed target. Despite seemingly trivial, this is a distinct formulation to OCP since the optimal policy typically varies at different initial state. Also notice that $\mathbf{X}_t \in \mathbb{R}^{B n_t}$ implies the dimension of \mathbf{X}_t (and \mathbf{P}_t) may change with time. This is a necessary extension to PMP since the dimension of the activation typically changes throughout layers to extract effective latent representation, yet it poses difficulties when one wish to adopt analysis from the continuous-time framework. Despite the recent attention on treating networks as an discretization of ODE [3, 9], we note that such formulation restricts the applicability of the optimal control theory to networks with residual architectures, as opposed to the generic dynamics we proposed here.

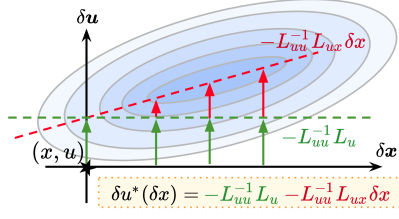


Table 2: Connection between existing algorithms and DDP

	1st-order	Adaptive 1st-order	Stage-wise Newton
Q_{uu}^{-1}	$\eta \mathbf{I}$	$\eta \text{diag}(\mathbf{g})$	J_{uu}^{-1}
Q_{ux}	$\mathbf{0}$	$\mathbf{0}$	$\mathbf{0}$

Figure 2: (Right) A toy illustration on the difference between the open and closed loop policy, denoted with green and red arrows. The feedback policy in this case is a line lying at the valley of objective L .

3.2 Trajectory Optimization Perspective

We now draw a new connection between the training procedure of DNNs and trajectory optimization. Let us first revisit the Back-propagation with gradient descent and adapt it with the notation appeared so far (see Alg. 2). During the forward propagation, we treat the weight as the *nominal control* $\bar{\mathbf{u}}$ that simulates the activation trajectory $\bar{\mathbf{x}}$. Then, the loss gradient is propagated backward, implicitly moving in the direction suggested by the Hamiltonian. The control update, in this case the first-order derivative, is computed simultaneously and later applied to the each layer.

It should be clear at this point that Alg. 2 resembles DDP in several ways. Starting from the same nominal trajectory, both algorithms carry certain information wrt the objective, either \mathbf{p}_t or (V_x^t, V_{xx}^t) , backward to compute the weight/control update. Since DDP also generates state-dependent feedback policies, additional forward simulation is required in order to apply the update. The computation graph for the two processes is summarized in Fig. 1. In the following proposition we make this connection formally and provide conditions when the two algorithms become equivalent.

Proposition 5. Assume $Q_{ux}^t = \mathbf{0}$ at all stages, then the backward dynamics of the value derivative can be described by the adjoint dynamics, i.e. $\forall t, V_x^t = \mathbf{p}_t$. Further, we have

$$Q_u^t = H_u^t = \nabla_{u_t} J, \quad \text{and} \quad Q_{uu}^t = \nabla_{u_t u_t} J. \quad (12)$$

In this case, the DDP algorithm is equivalent to the stage-wise Newton¹, i.e.

$$\delta u_t^*(\delta x_t) = -(Q_{uu}^t)^{-1} (Q_u^t + Q_{ux}^t \delta x_t) = -(\nabla_{u_t u_t} J)^{-1} \nabla_{u_t} J. \quad (13)$$

If further we have $Q_{uu}^t = \frac{1}{\eta} \mathbf{I}_{m_t}$, then DDP degenerates to Back-propagation with gradient descent.

Proof. See Appendix C.1. □

Proposition 5 states that the backward pass in DDP collapses to the Back-propagation when Q_{ux} vanishes. To better explain the role of Q_{ux} during optimization, consider an illustrated 2D example in Fig. 2. Given a differentiable objective L expanded at (x, u) , standard second-order methods compute its Hessian wrt u then apply the update $\delta u = -L_{uu}^{-1} L_u$ (shown as green arrow). DDP differs from them in that it also computes the *mixed* partial derivatives, i.e. L_{ux} . The resulting update law has the *same* intercept but with an additional feedback term linear in δx (shown as red arrow).

As for the role of feedback policies, first notice that the state differential has a compact expression written as $\delta x_t = \bar{f}_{t-1}(x_0, \bar{\mathbf{u}} + \delta \bar{\mathbf{u}}^*) - \bar{f}_{t-1}(x_0, \bar{\mathbf{u}})^2$. In the Appendix C.2 we further show that

$$\mathbf{K}_t \delta x_t \approx \arg \min_{\delta u_t \in \Gamma'(\delta x_t)} \|\nabla_{u_t} J(x_t + \delta x_t, u_t + \delta u_t) - \nabla_{u_t} J(x_t, u_t)\|, \quad (14)$$

where Γ' denote the set of all possible *affine* mappings. In other words, δx_t captures the state perturbation when new control is applied until layer t , and the feedback direction approximately minimizes the deviation of the gradients between perturbed and unperturbed states, i.e. $x_t^* \triangleq x_t + \delta x_t$ and x_t . We note that the difference between $\nabla_{u_t} J(x_t^*, u_t)$ and $\nabla_{u_t} J(x_t, u_t)$ cannot be neglected especially during early training when the objective landscape contains nontrivial curvature everywhere [31]. DDP feedback policies thus have a stabilization effect on robustifying the training dynamics.

¹ Stage-wise Newton precondition the gradient by the block-wise inverse Hessian at each layer.

² We denote $\bar{f}_{t-1} \triangleq f_{t-1} \circ \dots \circ f_0$ as the compositional dynamics propagating x_0 until time step t .

4 DDP Neural Optimizer for Feedforward Networks

In this section we discuss a practical implementation of DDP on training feedforward networks. Due to space constraint, we leave the complete derivation and full algorithm in the Appendix B.

Feedforward Network Dynamics: First, consider optimizing a single data point with DDP. This can be done by substituting the dynamics to the propagation rule of feedforward networks, i.e. by setting $f_t \equiv \sigma_t \circ g_t$ in Eq. (5). This will result in, take Q_u^t and Q_{uu}^t for instance, the following forms:

$$Q_u^t = \ell_u^t + g_u^t \top V_h^t, \quad Q_{uu}^t = \ell_{uu}^t + g_u^t \top (V_{hh}^t + V_x^{t+1} \cdot \sigma_{hh}^t) g_u^t + V_h^t \cdot g_{uu}^t, \quad (15)$$

where $V_h^t \triangleq \sigma_h^t \top V_{xx}^{t+1}$ and $V_{hh}^t \triangleq \sigma_h^t \top V_{xx}^{t+1} \sigma_h^t$ denote the derivatives of the value function wrt pre-activation h_t . Computing the feedback policy and value function remain the same as in Eq. (6, 7).

Batch DDP Training: Next, we augment the activation space to $X_t \in \mathbb{R}^{Bn_t}$ (recall B is the batch size) in the spirit of Proposition 4. We stress that despite drawing inspiration from the augmented Hamiltonian, the resulting batch DDP representation does not admit a clean form such as averaging over individual updates in Eq. (11). For instance, the derivative of batch-augmented value function at the prediction layer, denoted $V_{t'}(X_{t'})$ where $t' \equiv T-1$, admits a form of $V_X^{t'} = \frac{1}{B} [\cdots, \tilde{V}_{x^{(i)}}^{t'}, \cdots]^\top$, where $\tilde{V}_{x^{(i)}}^{t'}$ differs from $V_{x^{(i)}}^{t'}$ and, in fact, takes a much complicated form:

$$\tilde{V}_{x^{(i)}}^{t'} = Q_{x^{(i)}}^{t'} - Q_{x^{(i)}u}^{t'} (Q_{uu}^{t'})^{-1} Q_u^{t'}, \quad (16)$$

where $Q_u^{t'} = \frac{1}{B} \sum_i \nabla_u Q_{t'}(x_{t'}^{(i)}, u_{t'})$, $Q_{uu}^{t'} = \frac{1}{B} \sum_i \nabla_{uu} Q_{t'}(x_{t'}^{(i)}, u_{t'})$.

The intuition is that when optimizing batch trajectories with the *same* control law, the Bellman objective of each sample couples with others through the derivatives expansion related to u . Consequently, the value functions will no longer be independent soon after leaving the terminal horizon. We highlight this trait which distinguishes batch DDP from its original representation.

Curvature Approximation: Efficient curvature estimation of the loss landscape is particularly crucial in enabling the applicability of the second-order methods, since inverting the Hessian, even in a layer-wise fashion, can be computationally intractable, and DDP has no exception. Popular curvature factorization methods, such as KFAC [21] and its improved version EKfAC [22], rely on the fact that for feedforward layers, we have $J_{u_t} = g_u^t \top J_{h_t} = x_t \otimes J_{h_t}$, where \otimes denotes the Kronecker product. Thus, the Gauss-Newton (GN) approximation³ of $J_{u_t u_t}$ can be computed as

$$J_{u_t u_t} \approx \mathbb{E}[J_{u_t} J_{u_t}^\top] = \mathbb{E}[(x_t \otimes J_{h_t})(x_t \otimes J_{h_t})^\top] \approx \mathbb{E}[(x_t x_t^\top)] \otimes \mathbb{E}[(J_{h_t} J_{h_t}^\top)]. \quad (17)$$

The factorization in Eq. (17) is also applicable to DDP, as one can rewrite Eq. (15) with $g_u^t \top V_h^t = x_t \otimes V_h^t$. Following similar derivation, we will arrive at the Kronecker approximation of batch DDP:

$$Q_{uu}^t \approx \mathbb{E}[Q_u^t Q_u^{t \top}] = \mathbb{E}[(x_t \otimes V_h^t)(x_t \otimes V_h^t)^\top] \approx \mathbb{E}[x_t x_t^\top] \otimes \mathbb{E}[V_h^t V_h^{t \top}]. \quad (18)$$

Integrating DDP with existing optimizers is not restricted to second-order methods. Recall the connection we made in Sec. 3.2 and Table 2. When Q_{uu}^{-1} is isotropic, DDP inherits the same structure as gradient descent. In a similar vein, adaptive first order methods, such as RMSprop and Adam, approximate Q_{uu}^{-1} by $\text{diag}(g)$, where g adapting to the diagonal of the inverse covariance. Hereafter we will refer these integrations to DDP-SGD, DDP-RMSprop, and DDP-Adam. Second-order factorization using Eq. (18) will be referred to DDP-EKFAC. As a direct corollary from Proposition 5, we note that these algorithms will degenerate to the original baselines whenever all Q_{ux}^t vanish.

Regularization: We apply Tikhonov regularization on Q_{uu} and line search since both play key roles in the convergence of DDP [33]. These regularization have shown up already in training DNNs [34]. From the perspective of trajectory optimization, we note that without regularization, Q_{uu} will lose its positive definiteness whenever $g_u^t \top V_{xx}^{t+1} g_u^t$ has a low rank. This is indeed the case in feedforward networks. Similarly, when the dimension of the activation reduces during forward propagation, V_{xx}^t will also be low rank. Thus we also apply regularization to V_{xx}^t . Lastly, when using DDP for trajectory optimization, one typically has the option of expanding the dynamics up to first or second order. While both are still considered second-order methods and generate layer-wise feedback policies, the former performs GN approximation by omitting the tensor product of f_{xx}^t , f_{ux}^t , and f_{uu}^t in Eq. (5). The stability obtained by keeping only the linearized dynamics is discussed thoroughly in robotics literature [35, 36]. Thus, hereafter we will refer the DDP optimizer to this version.

³ If the network is viewed as exponential distribution, GN will be exactly the layer-wise Fisher matrix [32].

Table 3: Performance comparison on train loss and validation accuracy.
(+) and (-) respectively denote improvement and degradation over non-DDP algorithms.

	DataSet	SGD	RMSProp	Adam	KFAC	EKFAC	DDP SGD	DDP RMSProp	DDP Adam	DDP EKFAC	DDP
Training	WINE	0.565	0.552	0.557	0.560	0.561	0.566 (-)	0.552 (+)	0.557 (+)	0.561 (+)	0.565
	DIGITS	0.035	0.058	0.049	0.437	0.074	0.032 (+)	0.052 (+)	0.038 (+)	0.067 (+)	0.217
	MNIST	0.237	0.260	0.229	0.305	0.236	0.236 (+)	0.253 (+)	0.201 (+)	0.238 (-)	N/A
	FMNIST	0.471	0.433	0.416	0.470	0.433	0.475 (-)	0.430 (+)	0.393 (+)	0.429 (+)	N/A
Validate (%)	WINE	94.35	98.10	98.13	97.78	94.60	94.29 (-)	98.10 (+)	98.18 (+)	94.60 (+)	98.00
	DIGITS	95.36	94.33	94.98	85.55	95.24	95.52 (+)	94.63 (+)	95.13 (+)	95.19 (-)	91.68
	MNIST	92.65	91.89	92.54	91.95	92.73	92.63 (-)	91.97 (+)	93.30 (+)	92.61 (-)	N/A
	FMNIST	82.49	83.87	84.36	84.30	84.12	82.40 (-)	83.90 (+)	84.98 (+)	84.22 (+)	N/A

5 Experiments

Here we verify the performance of DDP optimizer on training (fully-connected) feedforward networks. The complete experiment setup and additional results are provided in the Appendix D. All values in tables and figures of this section are averaged over 10 seeds.

5.1 Performance on Synthetic and Classification Data Set

We first validate the DDP optimizer in batch trajectories optimization on a synthetic dataset, where we sample data from $k \in \{5, 8, 12, 15\}$ Gaussian clusters in \mathbb{R}^{30} . Since conceptually a DNN classifier can be thought of as a dynamical system guiding trajectories of samples toward the target regions belong to their classes, we hypothesize that for the DDP optimizer to show its effectiveness on batch training, the feedback policy must act as an ensemble policy that combines the locally optimal policy of each class. Fig. 3 shows the spectrum distribution, sorted in a descending order, of the feedback policy in the prediction layer. The result shows that the number of non-trivial eigenvalues matches exactly the number of classes in each setup (indicated by the vertical dashed line). As the distribution in the prediction layer concentrates to k bulks through training, the eigenvalues also increase, providing stronger feedback to the weight update. Thus, we consolidate our batch formulation in Sec. 4.

Next, we validate the performance of the DDP optimizer, along with several Hessian approximations proposed in the previous section, on classification tasks. In addition to the first-order baselines such as SGD, RMSprop [37], and Adam [38], we include state-of-the-art second order optimizers such as KFAC [21] and EKFAC [22]. We stress that all shared hyper-parameters (e.g. learning rate and weight decay) between optimizers and their DDP variants are kept the same, so that the performance gap only comes from DDP integration.

Table 3 summarizes the performance. On all data set, DDP-inspired algorithms achieve better results on both training and accuracy. Interestingly, notice first that when comparing the baseline methods with their DDP-integrated variants, the latter typically improve the convergence, especially for adaptive first-order methods. For instance, while Adam achieves comparable results among baselines on most dataset, DDP-Adam consistently outperforms Adam on *all* dataset. On the other hands, applying nontrivial curvature approximation to vanilla DDP, either using adaptive diagonal matrices or amortized Kronecker factorization in EKFAC, improves the training stability of DDP and its memory efficiency. In fact, we are not able to obtain result for vanilla DDP on (F)-MNIST due to the exploding computation when inverting Q_{uu}^t . These shed light on the benefit gained by bridging two seemingly disconnected methodologies between training deep nets and optimal control.

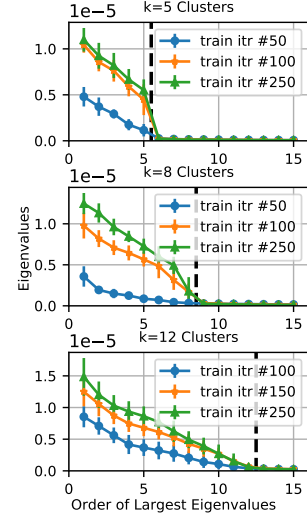


Figure 3: Spectrum distribution on synthetic dataset.

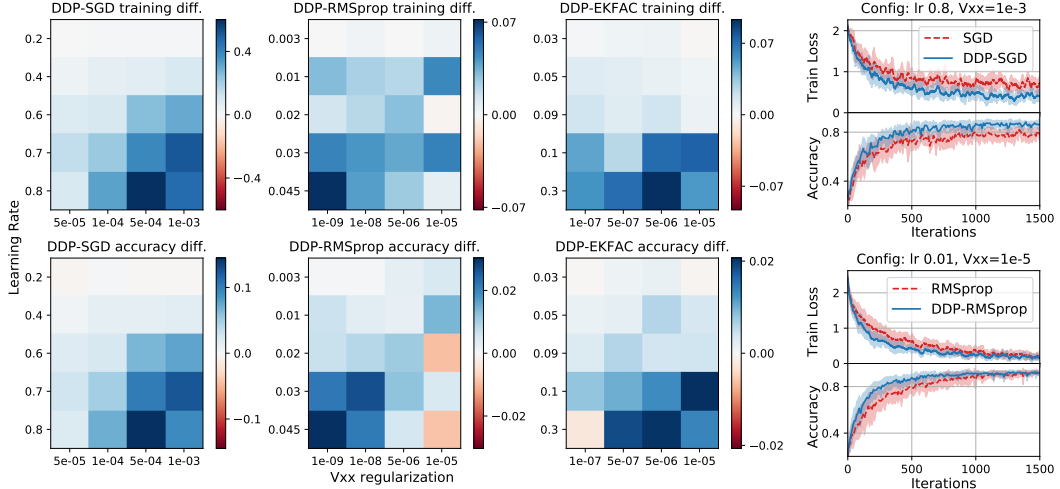


Figure 4: (a) Analysis of performance difference between DDP and baselines on DIGITS across hyper-parameter grid, with blue (resp. red) indicating improvement (resp. degradation) over baselines. The color bars are scaled for best view. (b) Two examples of the actual training and accuracy curves.

5.2 Analysis on Feedback Policies

To identify scenarios where the feedback mechanism best show its effectiveness, we compare the performance difference between baselines and their DDP-integrated variants over different learning rate and V_{xx} regularization. Similar to Sec. 5.1, we keep all the other hyper-parameters the same. The result is shown in Fig. 4a, where each grid corresponds to a distinct configuration. Blue (resp. red) indicates improvement (resp. degradation) when the feedback policies are presented. While the improvement of baselines with the DDP integration remains consistent across most hyper-parameters setups, the performance gap tends to become obvious as the learning rate increases. This suggests DDP has an effect of robustifying the unstable training dynamics when a further step size, i.e. a larger control value, is taken. As shown in Fig. 4b, such a stabilization can also lead to smaller variance and faster (sometimes better) convergence.

Lastly, we present an interesting finding on how the feedback policies help mitigate vanishing gradient (VG), a notorious effect when DNNs become impossible to train as the gradient vanishes along the Back-propagation. Fig. 5 reports results on training a 9-layers sigmoid-activated DNN on DIGITS. While the second-order baseline, i.e. EKFAC, suffers to make any progress as J_{u_t} , together with its Kronecker factorization, vanish along Back-propagation, DDP-EKFAC continues to provide training signal as the state-dependent feedback, i.e. $\mathbf{K}_t \delta \mathbf{x}_t$, remains active. The effect becomes significant when dynamics is fully expanded to second order. As shown in Fig. 5, the update norm from DDP-EKFAC is typically 5-10 times larger than EKFAC. We note that in this experiment, we replace the cross-entropy (CE) loss with Max-Mahalanobis center (MMC) loss, a new classification objective that improves robustness on standard vision dataset [39]. MMC casts classification to distributional regression, providing denser Hessian and making problem similar to original trajectory optimization. None of the algorithms escape from VG using CE loss. We highlight that while VG is typically mitigated on the *architecture* basis, by having either unbounded activation function or residual blocks, the DDP framework provides an alternative from the *algorithmic* perspective.

Conclusion: In this work, we introduce Differential Dynamic Programming neural optimizer, a new class of algorithms arising from bridging DNNs training to the optimal control and trajectory optimization. This new perspective suggests existing methods stand as special cases of DDP and can be extended to adapt the framework. The resulting optimizer features layer-wise feedback policies which help improve training convergence and robustness to hyper-parameters. We wish this work provides new algorithmic insight and bridges between deep learning and optimal control.

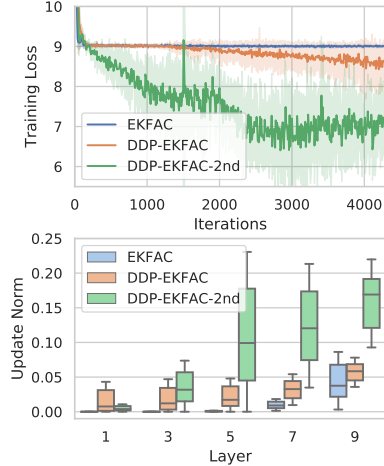


Figure 5: Training a 9-layer sigmoid-activated network on DIGITS, using MMC loss [39].

Broader Impact

We believe the Broader Impact on ethical or societal aspects is not directly applicable to this work, as we focus primarily on exploring the theoretic connection between deep learning and optimal control theory, the two previously disjointed methodologies that have attracted considerable attention recently in fundamental understanding of deep neural networks. Our work strengthens the relation, and from such proposes a new class of algorithm for a general optimization purpose.

At a high level, (optimal) control theory is a relatively mature research area, whose applications appear from automating manufacture to trajectory optimization of the humanoid robotics. Since reliability typically stands as key matrices for industrial applications, control-theoretic viewpoint provides rich analysis on the robustness and stability of the system. As the machine learning community gathers interests in improving the robustness of deep models from security and reproducibility standpoints, we hope this work makes an attempt along this line by bringing control-theoretic analysis to the community.

Acknowledgments

The authors would like to thank Chen-Hsuan Lin, Yen-Cheng Liu, and Chia-Wen Kuo for many helpful discussions on the paper. The work is supported under Amazon AWS Machine Learning Research Award (MLRA).

References

- [1] E Weinan. A proposal on machine learning via dynamical systems. *Communications in Mathematics and Statistics*, 5(1):1–11, 2017.
- [2] Yiping Lu, Zhuohan Li, Di He, Zhiqing Sun, Bin Dong, Tao Qin, Liwei Wang, and Tie-Yan Liu. Understanding and improving transformer from a multi-particle dynamic system point of view. *arXiv preprint arXiv:1906.02762*, 2019.
- [3] Yiping Lu, Aoxiao Zhong, Quanzheng Li, and Bin Dong. Beyond finite layer neural networks: Bridging deep architectures and numerical differential equations. *arXiv preprint arXiv:1710.10121*, 2017.
- [4] Zichao Long, Yiping Lu, Xianzhong Ma, and Bin Dong. Pde-net: Learning pdes from data. *arXiv preprint arXiv:1710.09668*, 2017.
- [5] Samuel Greydanus, Misko Dzamba, and Jason Yosinski. Hamiltonian neural networks. In *Advances in Neural Information Processing Systems*, pages 15353–15363, 2019.
- [6] Yaofeng Desmond Zhong, Biswadip Dey, and Amit Chakraborty. Symplectic ode-net: Learning hamiltonian dynamics with control. *arXiv preprint arXiv:1909.12077*, 2019.
- [7] Tian Qi Chen, Yulia Rubanova, Jesse Bettencourt, and David K Duvenaud. Neural ordinary differential equations. In *Advances in Neural Information Processing Systems*, pages 6572–6583, 2018.
- [8] Xuanqing Liu, Tesi Xiao, Si Si, Qin Cao, Sanjiv Kumar, and Cho-Jui Hsieh. Neural sde: Stabilizing neural ode networks with stochastic noise. *arXiv preprint arXiv:1906.02355*, 2019.
- [9] E Weinan, Jiequn Han, and Qianxiao Li. A mean-field optimal control formulation of deep learning. *arXiv preprint arXiv:1807.01083*, 2018.
- [10] Jacob H Seidman, Mahyar Fazlyab, Victor M Preciado, and George J Pappas. Robust deep learning as optimal control: Insights and convergence guarantees. *Proceedings of Machine Learning Research vol xxx*, 1:14, 2020.
- [11] Guan-Horng Liu and Evangelos A Theodorou. Deep learning theory review: An optimal control and dynamical systems perspective. *arXiv preprint arXiv:1908.10920*, 2019.
- [12] Vladimir Grigor’evich Boltyanskii, Revaz Valer’yanovich Gamkrelidze, and Lev Semenovich Pontryagin. The theory of optimal processes. i. the maximum principle. Technical report, TRW SPACE TECHNOLOGY LABS LOS ANGELES CALIF, 1960.

- [13] Stefanie Gunther, Lars Ruthotto, Jacob B Schroder, Eric C Cyr, and Nicolas R Gauger. Layer-parallel training of deep residual neural networks. *SIAM Journal on Mathematics of Data Science*, 2(1):1–23, 2020.
- [14] Qianxiao Li and Shuji Hao. An optimal control approach to deep learning and applications to discrete-weight neural networks. *arXiv preprint arXiv:1803.01299*, 2018.
- [15] Qianxiao Li, Long Chen, Cheng Tai, and E Weinan. Maximum principle based algorithms for deep learning. *The Journal of Machine Learning Research*, 18(1):5998–6026, 2017.
- [16] Dimitri P Bertsekas, Dimitri P Bertsekas, Dimitri P Bertsekas, and Dimitri P Bertsekas. *Dynamic programming and optimal control*. Athena scientific Belmont, MA, 1995.
- [17] Li-zhi Liao and Christine A Shoemaker. Advantages of differential dynamic programming over newton’s method for discrete-time optimal control problems. Technical report, Cornell University, 1992.
- [18] D.H. Jacobson and D.Q. Mayne. *Differential Dynamic Programming*. Modern analytic and computational methods in science and mathematics. American Elsevier Publishing Company, 1970. URL <https://books.google.com/books?id=tA-oAAAAIAAJ>.
- [19] Yuval Tassa, Nicolas Mansard, and Emo Todorov. Control-limited differential dynamic programming. In *2014 IEEE International Conference on Robotics and Automation (ICRA)*, pages 1168–1175. IEEE, 2014.
- [20] Michael Posa, Scott Kuindersma, and Russ Tedrake. Optimization and stabilization of trajectories for constrained dynamical systems. In *2016 IEEE International Conference on Robotics and Automation (ICRA)*, pages 1366–1373. IEEE, 2016.
- [21] James Martens and Roger Grosse. Optimizing neural networks with kronecker-factored approximate curvature. In *International conference on machine learning*, pages 2408–2417, 2015.
- [22] Thomas George, César Laurent, Xavier Bouthillier, Nicolas Ballas, and Pascal Vincent. Fast approximate natural gradient descent in a kronecker factored eigenbasis. In *Advances in Neural Information Processing Systems*, pages 9550–9560, 2018.
- [23] Junyoung Chung, Caglar Gulcehre, Kyunghyun Cho, and Yoshua Bengio. Gated feedback recurrent neural networks. In *International conference on machine learning*, pages 2067–2075, 2015.
- [24] Haiguang Wen, Kuan Han, Junxing Shi, Yizhen Zhang, Eugenio Culurciello, and Zhongming Liu. Deep predictive coding network for object recognition. *arXiv preprint arXiv:1802.04762*, 2018.
- [25] Amir R Zamir, Te-Lin Wu, Lin Sun, William B Shen, Bertram E Shi, Jitendra Malik, and Silvio Savarese. Feedback networks. In *Proceedings of the IEEE Conference on Computer Vision and Pattern Recognition*, pages 1308–1317, 2017.
- [26] Zhen Li, Jinglei Yang, Zheng Liu, Xiaomin Yang, Gwanggil Jeon, and Wei Wu. Feedback network for image super-resolution. In *Proceedings of the IEEE Conference on Computer Vision and Pattern Recognition*, pages 3867–3876, 2019.
- [27] Firas Shama, Roey Mechrez, Alon Shoshan, and Lihi Zelnik-Manor. Adversarial feedback loop. In *Proceedings of the IEEE International Conference on Computer Vision*, pages 3205–3214, 2019.
- [28] Minyoung Huh, Shao-Hua Sun, and Ning Zhang. Feedback adversarial learning: Spatial feedback for improving generative adversarial networks. In *Proceedings of the IEEE Conference on Computer Vision and Pattern Recognition*, pages 1476–1485, 2019.
- [29] Emanuel Todorov. Optimal control theory. *Bayesian brain: probabilistic approaches to neural coding*, pages 269–298, 2016.
- [30] Richard Bellman. The theory of dynamic programming. Technical report, Rand corp santa monica ca, 1954.
- [31] Guillaume Alain, Nicolas Le Roux, and Pierre-Antoine Manzagol. Negative eigenvalues of the hessian in deep neural networks. *arXiv preprint arXiv:1902.02366*, 2019.
- [32] James Martens. New insights and perspectives on the natural gradient method. *arXiv preprint arXiv:1412.1193*, 2014.

- [33] L-Z Liao and Christine A Shoemaker. Convergence in unconstrained discrete-time differential dynamic programming. *IEEE Transactions on Automatic Control*, 36(6):692–706, 1991.
- [34] Sharan Vaswani, Aaron Mishkin, Issam Laradji, Mark Schmidt, Gauthier Gidel, and Simon Lacoste-Julien. Painless stochastic gradient: Interpolation, line-search, and convergence rates. In *Advances in Neural Information Processing Systems*, pages 3727–3740, 2019.
- [35] Emanuel Todorov and Weiwei Li. A generalized iterative lqg method for locally-optimal feedback control of constrained nonlinear stochastic systems. In *Proceedings of the 2005, American Control Conference, 2005.*, pages 300–306. IEEE, 2005.
- [36] Yuval Tassa, Tom Erez, and Emanuel Todorov. Synthesis and stabilization of complex behaviors through online trajectory optimization. In *2012 IEEE/RSJ International Conference on Intelligent Robots and Systems*, pages 4906–4913. IEEE, 2012.
- [37] Geoffrey Hinton, Nitish Srivastava, and Kevin Swersky. Neural networks for machine learning lecture 6a overview of mini-batch gradient descent. 2012.
- [38] Diederik P Kingma and Jimmy Ba. Adam: A method for stochastic optimization. *arXiv preprint arXiv:1412.6980*, 2014.
- [39] Tianyu Pang, Kun Xu, Yinpeng Dong, Chao Du, Ning Chen, and Jun Zhu. Rethinking softmax cross-entropy loss for adversarial robustness. *arXiv preprint arXiv:1905.10626*, 2019.

Supplementary Material

A Derivation of Batch PMP

A.1 Problem Formulation and Notation

Recall the original OCP for single trajectory optimization. In its batch setting, we consider the following state-augmented optimal control problem:

$$\min_{\bar{\mathbf{u}}} \mathbf{J}(\bar{\mathbf{u}}; \mathbf{X}_0) := \left[\Phi(\mathbf{X}_T) + \sum_{t=0}^{T-1} \mathbf{L}_t(\mathbf{X}_t, \mathbf{u}_t) \right], \quad \text{s.t. } \mathbf{X}_{t+1} = \mathbf{F}_t(\mathbf{X}_t, \mathbf{u}_t), \quad (19)$$

where $\mathbf{X}_t \triangleq [\dots \mathbf{x}_t^{(i)\top} \dots]^\top \in \mathbb{R}^{Bn_t}$ denotes the state-augmented vector over each $\mathbf{x}_t^{(i)} \in \mathbb{R}^{n_t}$. B denotes the batch size. $\mathbf{L}_t(\mathbf{X}_t, \mathbf{u}_t)$ and $\Phi(\mathbf{X}_T)$ respectively represent the average intermediate and terminal cost over $\ell_t(\mathbf{x}_t^{(i)}, \mathbf{u}_t)$ and $\phi(\mathbf{x}_T^{(i)})$. \mathbf{F}_t consists of B independent mappings from each dynamics $f_t(\mathbf{x}_t^{(i)}, \cdot)$. Consequently, its derivatives can be related to the ones for each sample by

$$\begin{aligned} \nabla_{\mathbf{u}_t} \mathbf{F}_t(\mathbf{X}_t, \mathbf{u}_t) &\equiv \mathbf{F}_{\mathbf{u}}^t \in \mathbb{R}^{Bn_{t'} \times m_t}, & \text{where } [\mathbf{F}_{\mathbf{u}}^t]_{(B_{n_{t'}^{(i)}}, :)} &= f_{\mathbf{u}}^t|^{(i)} \\ \nabla_{\mathbf{X}_t} \mathbf{F}_t(\mathbf{X}_t, \mathbf{u}_t) &\equiv \mathbf{F}_{\mathbf{X}}^t \in \mathbb{R}^{Bn_{t'} \times Bn_t}, & \text{where } [\mathbf{F}_{\mathbf{X}}^t]_{(B_{n_{t'}^{(i)}}, B_{n_t^{(j)}})} &= \delta_{ij} f_{\mathbf{x}}^t|^{(i)}, \\ \nabla_{\mathbf{u}_t \mathbf{X}_t} \mathbf{F}_t(\mathbf{X}_t, \mathbf{u}_t) &\equiv \mathbf{F}_{\mathbf{uX}}^t \in \mathbb{R}^{Bn_{t'} \times m_t \times Bn_t}, & \text{where } [\mathbf{F}_{\mathbf{uX}}^t]_{(B_{n_{t'}^{(i)}}, :, B_{n_t^{(j)}})} &= \delta_{ij} f_{\mathbf{uX}}^t|^{(i)}, \\ \nabla_{\mathbf{X}_t \mathbf{X}_t} \mathbf{F}_t(\mathbf{X}_t, \mathbf{u}_t) &\equiv \mathbf{F}_{\mathbf{XX}}^t \in \mathbb{R}^{Bn_{t'} \times Bn_t \times Bn_t}, & \text{where } [\mathbf{F}_{\mathbf{XX}}^t]_{(B_{n_{t'}^{(i)}}, B_{n_t^{(j)}}, B_{n_t^{(k)}})} &= \delta_{ijk} f_{\mathbf{XX}}^t|^{(i)}, \\ \nabla_{\mathbf{u}_t \mathbf{u}_t} \mathbf{F}_t(\mathbf{X}_t, \mathbf{u}_t) &\equiv \mathbf{F}_{\mathbf{uu}}^t \in \mathbb{R}^{Bn_{t'} \times m_t \times m_t}, & \text{where } [\mathbf{F}_{\mathbf{uu}}^t]_{(B_{n_{t'}^{(i)}}, :, :)} &= f_{\mathbf{uu}}^t|^{(i)}. \end{aligned} \quad (20)$$

δ_{ij} and δ_{ijk} represent the Kronecker delta. For simplicity, we denote $t' \triangleq t+1$ and $B_d^{(i)} \triangleq ((i-1)d : id)$ as the indices for i -th block, each with the dimension d . $f_{\mathbf{uX}}^t|^{(i)} \triangleq \nabla_{\mathbf{u}_t \mathbf{x}_t} f_t(\mathbf{x}_t^{(i)}, \mathbf{u}_t)$ represents the derivative of the dynamics of the sample i . Notice again that t appears in the subscript of the gradient since we allow the dimension of \mathbf{X}_t to change at each layer.

A.2 Formal Statement for Proposition 4

Proposition 6. *Let $\bar{\mathbf{u}}^*$ be the optimal control trajectory for the augmented problem described in Eq. (19) and $\bar{\mathbf{X}}^*$ be the corresponding augmented state trajectory. Then, there exists a co-state trajectory $\bar{\mathbf{P}}^* \triangleq \{\mathbf{P}_t^*\}_{t=1}^T$, such that the following ‘augmented’ PMP equations are satisfied:*

$$\mathbf{X}_{t+1}^* = \nabla_{\mathbf{P}_{t+1}} \mathbf{H}_t(\mathbf{X}_t^*, \mathbf{P}_{t+1}^*, \mathbf{u}_t^*), \quad \mathbf{X}_0^* = \mathbf{X}_0, \quad (21a)$$

$$\mathbf{P}_t^* = \nabla_{\mathbf{X}_t} \mathbf{H}_t(\mathbf{X}_t^*, \mathbf{P}_{t+1}^*, \mathbf{u}_t^*), \quad \mathbf{P}_T^* = \nabla_{\mathbf{X}_T} \Phi(\mathbf{X}_T^*), \quad (21b)$$

$$\mathbf{u}_t^* = \arg \min_{\mathbf{v}} \mathbf{H}_t(\mathbf{X}_t^*, \mathbf{P}_{t+1}^*, \mathbf{v}), \quad \forall \mathbf{v} \in \mathbb{R}^{m_t}, \quad (21c)$$

where the augmented Hamiltonian $\mathbf{H}_t : \mathbb{R}^{Bn_t} \times \mathbb{R}^{Bn_{t+1}} \times \mathbb{R}^{m_t} \mapsto \mathbb{R}$ at each time step is given by

$$\mathbf{H}_t(\mathbf{X}_t, \mathbf{P}_{t+1}, \mathbf{u}_t) = \mathbf{P}_{t+1}^\top \mathbf{F}_t(\mathbf{X}_t, \mathbf{u}_t) + \mathbf{L}_t(\mathbf{X}_t, \mathbf{u}_t). \quad (22)$$

Furthermore, solving Eq. (21c) iteratively by $\mathbf{u}_t^{(k+1)} = \mathbf{u}_t^{(k)} - \eta \nabla_{\mathbf{u}_t} \mathbf{H}_t(\mathbf{X}_t, \mathbf{P}_{t+1}, \mathbf{u}_t^{(k)})$ is equivalent to applying mini-batch gradient descent with Back-propagation.

Proof. It is obvious to see that Eq. (21a) forward propagates each $\mathbf{x}_t^{(i)}$. To bridge Eq. (21b) to the mini-batch Back-propagation, we first notice that the augmented co-state at the terminal time admits a simple form:

$$\mathbf{P}_T = \nabla_{\mathbf{X}_T} \Phi(\mathbf{X}_T) = \frac{1}{B} \begin{bmatrix} \nabla_{\mathbf{x}_T} \phi(\mathbf{x}_T^{(1)}) \\ \vdots \\ \nabla_{\mathbf{x}_T} \phi(\mathbf{x}_T^{(B)}) \end{bmatrix} = \frac{1}{B} \begin{bmatrix} \mathbf{p}_T^{(1)} \\ \vdots \\ \mathbf{p}_T^{(B)} \end{bmatrix}. \quad (23)$$

In other words, \mathbf{P}_T is a collection over each co-state $\mathbf{p}_T^{(i)}$ and normalizes by the batch size. We can show by induction that such a structure is preserved throughout the adjoint dynamics in Eq. (21b):

$$\begin{aligned} \mathbf{P}_t &= \nabla_{\mathbf{X}_t} \mathbf{H}_t(\mathbf{X}_t, \mathbf{P}_{t+1}, \mathbf{u}_t) \\ &= \mathbf{L}_{\mathbf{X}}^t + \mathbf{F}_{\mathbf{X}}^t{}^\top \mathbf{P}_{t+1} \\ &= \frac{1}{B} \begin{bmatrix} \nabla_{\mathbf{x}_t} \ell_t(\mathbf{x}_t^{(1)}, \mathbf{u}_t) + \nabla_{\mathbf{x}_t} f_t(\mathbf{x}_t^{(1)}, \mathbf{u}_t)^\top \mathbf{p}_{t+1}^{(1)} \\ \vdots \\ \nabla_{\mathbf{x}_t} \ell_t(\mathbf{x}_t^{(B)}, \mathbf{u}_t) + \nabla_{\mathbf{x}_t} f_t(\mathbf{x}_t^{(B)}, \mathbf{u}_t)^\top \mathbf{p}_{t+1}^{(B)} \end{bmatrix} = \frac{1}{B} \begin{bmatrix} \mathbf{p}_t^{(1)} \\ \vdots \\ \mathbf{p}_t^{(B)} \end{bmatrix}. \end{aligned} \quad (24)$$

Finally, the update direction is given by

$$\begin{aligned} \nabla_{\mathbf{u}_t} \mathbf{H}_t(\mathbf{X}_t, \mathbf{P}_{t+1}, \mathbf{u}_t) &= \mathbf{L}_{\mathbf{u}}^t + \mathbf{F}_{\mathbf{u}}^t{}^\top \mathbf{P}_{t+1} \\ &= \frac{1}{B} \sum_i \nabla_{\mathbf{u}_t} \ell_t(\mathbf{x}_t^{(i)}, \mathbf{u}_t) + \frac{1}{B} \sum_i [\mathbf{F}_{\mathbf{u}}^t]_{(B^{n_{t+1}}, :)}^\top \mathbf{p}_{t+1}^{(i)} \\ &= \frac{1}{B} \sum_i \nabla_{\mathbf{u}_t} \ell_t(\mathbf{x}_t^{(i)}, \mathbf{u}_t) + \nabla_{\mathbf{u}_t} f_t(\mathbf{x}_t^{(i)}, \mathbf{u}_t)^\top \mathbf{p}_{t+1}^{(i)} \\ &= \frac{1}{B} \sum_i \nabla_{\mathbf{u}_t} H(\mathbf{x}_t^{(i)}, \mathbf{u}_t, \mathbf{p}_{t+1}^{(i)}) = \frac{1}{B} \sum_i \nabla_{\mathbf{u}_t} J(\mathbf{u}_t; \mathbf{x}_0^{(i)}), \end{aligned} \quad (25)$$

which is the exact mini-batch gradient update. \square

Remarks: It should be stressed that the relation between \mathbf{P}_t and \mathbf{p}_t by simply taking the average is only true when first-order derivatives are involved. In Appendix B.2, we will show that the backward pass for the augmented value function does not admit this property and therefore can be much complex.

B Derivation of Batch DDP for Feedforward Networks

In this part we provide the complete derivation in Sec. 4 for optimizing feedforward networks with batch DDP optimizer.

B.1 Feedforward Networks as Dynamical Systems

We first consider the original DDP formulation when feedforward networks are used as dynamics. Here we provide derivations for the new δQ_t expansion and how it can be computed efficiently.

Derivation of Eq. (15).

$$\begin{aligned} Q_{\mathbf{u}} &= \ell_{\mathbf{u}} + f_{\mathbf{u}}^\top V'_{\mathbf{x}'} = \ell_{\mathbf{u}} + g_{\mathbf{u}}^\top \sigma_{\mathbf{h}}^\top V'_{\mathbf{x}'}, \\ Q_{\mathbf{u}\mathbf{u}} &= \ell_{\mathbf{u}\mathbf{u}} + \frac{\partial}{\partial \mathbf{u}} \{g_{\mathbf{u}}^\top \sigma_{\mathbf{h}}^\top V'_{\mathbf{x}'}\} \\ &= \ell_{\mathbf{u}\mathbf{u}} + g_{\mathbf{u}}^\top \sigma_{\mathbf{h}}^\top \frac{\partial}{\partial \mathbf{u}} \{V'_{\mathbf{x}'}\} + g_{\mathbf{u}}^\top \left(\frac{\partial}{\partial \mathbf{u}} \{\sigma_{\mathbf{h}}\} \right)^\top V'_{\mathbf{x}'} + \left(\frac{\partial}{\partial \mathbf{u}} \{g_{\mathbf{u}}\} \right)^\top \sigma_{\mathbf{h}}^\top V'_{\mathbf{x}'}, \\ &= \ell_{\mathbf{u}\mathbf{u}} + g_{\mathbf{u}}^\top \sigma_{\mathbf{h}}^\top V'_{\mathbf{x}'\mathbf{x}'} \sigma_{\mathbf{h}} g_{\mathbf{u}} + g_{\mathbf{u}}^\top (V'_{\mathbf{x}'}{}^\top \sigma_{\mathbf{h}\mathbf{h}} g_{\mathbf{u}}) + g_{\mathbf{u}\mathbf{u}}^\top \sigma_{\mathbf{h}}^\top V'_{\mathbf{x}'}, \\ &= \ell_{\mathbf{u}\mathbf{u}} + g_{\mathbf{u}}^\top (V_{\mathbf{h}\mathbf{h}} + V'_{\mathbf{x}'} \cdot \sigma_{\mathbf{h}\mathbf{h}}) g_{\mathbf{u}} + V_{\mathbf{h}} \cdot g_{\mathbf{u}\mathbf{u}} \end{aligned}$$

The last equation follows by recalling $V_{\mathbf{h}} \triangleq \sigma_{\mathbf{h}}^\top V'_{\mathbf{x}'}$, and $V_{\mathbf{h}\mathbf{h}} \triangleq \sigma_{\mathbf{h}}^\top V'_{\mathbf{x}'\mathbf{x}'} \sigma_{\mathbf{h}}$. Note that we drop the superscript t for notational simplicity and denote $V'_{\mathbf{x}'} \triangleq \nabla_{\mathbf{x}} V_{t+1}(\mathbf{x}_{t+1})$ as the derivative of the value function at the next state. Follow similar derivation, we have

$$\begin{aligned} Q_{\mathbf{x}} &= \ell_{\mathbf{x}} + g_{\mathbf{x}}^\top V_{\mathbf{h}} \\ Q_{\mathbf{x}\mathbf{x}} &= \ell_{\mathbf{x}\mathbf{x}} + g_{\mathbf{x}}^\top (V_{\mathbf{h}\mathbf{h}} + V'_{\mathbf{x}'} \cdot \sigma_{\mathbf{h}\mathbf{h}}) g_{\mathbf{x}} + V_{\mathbf{h}} \cdot g_{\mathbf{x}\mathbf{x}} \\ Q_{\mathbf{u}\mathbf{x}} &= \ell_{\mathbf{u}\mathbf{x}} + g_{\mathbf{u}}^\top (V_{\mathbf{h}\mathbf{h}} + V'_{\mathbf{x}'} \cdot \sigma_{\mathbf{h}\mathbf{h}}) g_{\mathbf{x}} + V_{\mathbf{h}} \cdot g_{\mathbf{u}\mathbf{x}} \end{aligned} \quad (26)$$

Remarks: The computational overhead in Eq. (15, 26) can be mitigated by leveraging the structure of feedforward networks. Since the affine transform is bilinear in \mathbf{x}_t and \mathbf{u}_t , the terms $g_{\mathbf{x}\mathbf{x}}^t$ and $g_{\mathbf{u}\mathbf{u}}^t$

vanish. The tensor $g_{\mathbf{u}\mathbf{x}}^t$ admits a sparse structure. For fully-connected layers, computation can be simplified to

$$\begin{aligned} [g_{\mathbf{u}\mathbf{x}}^t]_{(i,j,k)} &= 1 \quad \text{iff} \quad j = (k-1)n_{t+1} + i, \\ [V_{\mathbf{h}}^t \cdot g_{\mathbf{u}\mathbf{x}}^t]_{((k-1)n_{t+1}:kn_{t+1},k)} &= V_{\mathbf{h}}^t. \end{aligned} \quad (27)$$

For the coordinate-wise nonlinear transform, $\sigma_{\mathbf{h}}^t$ and $\sigma_{\mathbf{h}\mathbf{h}}^t$ are diagonal matrix and tensor. In most learning instances, stage-wise losses typically involved with weight decay alone; thus the terms $\ell_{\mathbf{x}}^t, \ell_{\mathbf{x}\mathbf{x}}^t, \ell_{\mathbf{u}\mathbf{x}}^t$ also vanish.

B.2 Batch DDP Formulation

Next, we extend the formulation in Appendix B.1 to the batch setting by adopting the same notation in Appendix A.1. Given the augmented Bellman objective $\mathbf{Q}(\mathbf{X}_t, \mathbf{u}_t) \triangleq \mathbf{L}_t(\mathbf{X}_t, \mathbf{u}_t) + \mathbf{V}_{t+1}(\mathbf{F}_t(\mathbf{X}_t, \mathbf{u}_t))$, we modify Eq. (15) by substituting $\mathbf{F}_t \equiv \sigma_t \circ \mathbf{G}_t$,

$$\mathbf{Q}_{\mathbf{X}}^t = \mathbf{L}_{\mathbf{X}}^t + \mathbf{F}_{\mathbf{X}}^{t\top} \mathbf{V}_{\mathbf{X}'}^t = \mathbf{L}_{\mathbf{X}}^t + \mathbf{G}_{\mathbf{X}}^{t\top} \mathbf{V}_{\mathbf{H}}^t \quad (28a)$$

$$\mathbf{Q}_{\mathbf{u}}^t = \mathbf{L}_{\mathbf{u}}^t + \mathbf{F}_{\mathbf{u}}^{t\top} \mathbf{V}_{\mathbf{X}'}^t = \mathbf{L}_{\mathbf{u}}^t + \mathbf{G}_{\mathbf{u}}^{t\top} \mathbf{V}_{\mathbf{H}}^t \quad (28b)$$

$$\begin{aligned} \mathbf{Q}_{\mathbf{X}\mathbf{X}}^t &= \mathbf{L}_{\mathbf{X}\mathbf{X}}^t + \mathbf{F}_{\mathbf{X}}^{t\top} \mathbf{V}_{\mathbf{X}'\mathbf{X}'}^t \mathbf{F}_{\mathbf{X}}^t + \mathbf{V}_{\mathbf{X}'}^t \cdot \mathbf{F}_{\mathbf{X}\mathbf{X}}^t \\ &= \mathbf{L}_{\mathbf{X}\mathbf{X}}^t + \mathbf{G}_{\mathbf{X}}^{t\top} (\mathbf{V}_{\mathbf{H}\mathbf{H}}^t + \mathbf{V}_{\mathbf{X}'}^t \cdot \sigma_{\mathbf{H}\mathbf{H}}^t) \mathbf{G}_{\mathbf{X}}^t + \mathbf{V}_{\mathbf{H}}^t \cdot \mathbf{G}_{\mathbf{X}\mathbf{X}}^t \end{aligned} \quad (28c)$$

$$\begin{aligned} \mathbf{Q}_{\mathbf{u}\mathbf{u}}^t &= \mathbf{L}_{\mathbf{u}\mathbf{u}}^t + \mathbf{F}_{\mathbf{u}}^{t\top} \mathbf{V}_{\mathbf{X}'\mathbf{X}'}^t \mathbf{F}_{\mathbf{u}}^t + \mathbf{V}_{\mathbf{X}'}^t \cdot \mathbf{F}_{\mathbf{u}\mathbf{u}}^t \\ &= \mathbf{L}_{\mathbf{u}\mathbf{u}}^t + \mathbf{G}_{\mathbf{u}}^{t\top} (\mathbf{V}_{\mathbf{H}\mathbf{H}}^t + \mathbf{V}_{\mathbf{X}'}^t \cdot \sigma_{\mathbf{H}\mathbf{H}}^t) \mathbf{G}_{\mathbf{u}}^t + \mathbf{V}_{\mathbf{H}}^t \cdot \mathbf{G}_{\mathbf{u}\mathbf{u}}^t \end{aligned} \quad (28d)$$

$$\begin{aligned} \mathbf{Q}_{\mathbf{u}\mathbf{X}}^t &= \mathbf{L}_{\mathbf{u}\mathbf{X}}^t + \mathbf{F}_{\mathbf{u}}^{t\top} \mathbf{V}_{\mathbf{X}'\mathbf{X}'}^t \mathbf{F}_{\mathbf{X}}^t + \mathbf{V}_{\mathbf{X}'}^t \cdot \mathbf{F}_{\mathbf{u}\mathbf{X}}^t \\ &= \mathbf{L}_{\mathbf{u}\mathbf{X}}^t + \mathbf{G}_{\mathbf{u}}^{t\top} (\mathbf{V}_{\mathbf{H}\mathbf{H}}^t + \mathbf{V}_{\mathbf{X}'}^t \cdot \sigma_{\mathbf{H}\mathbf{H}}^t) \mathbf{G}_{\mathbf{X}}^t + \mathbf{V}_{\mathbf{H}}^t \cdot \mathbf{G}_{\mathbf{u}\mathbf{X}}^t, \end{aligned} \quad (28e)$$

where $\mathbf{V}_{\mathbf{H}}^t$ and $\mathbf{V}_{\mathbf{H}\mathbf{H}}^t$ are given by

$$\mathbf{V}_{\mathbf{H}}^t \triangleq \sigma_{\mathbf{H}}^{t\top} \mathbf{V}_{\mathbf{X}'}^t, \quad \mathbf{V}_{\mathbf{H}\mathbf{H}}^t \triangleq \sigma_{\mathbf{H}}^{t\top} \mathbf{V}_{\mathbf{X}'\mathbf{X}'}^t \sigma_{\mathbf{H}}^t. \quad (29)$$

Once we have all the \mathbf{Q} derivatives explicitly written, computing layer-wise feedback policies and backward passing the derivatives of the augmented value follow by the same equations as in the original DDP, i.e.

$$\delta \mathbf{u}_t^*(\delta \mathbf{X}_t) = \bar{\mathbf{k}}_t + \bar{\mathbf{K}}_t \delta \mathbf{X}_t = -(\mathbf{Q}_{\mathbf{u}\mathbf{u}}^t)^{-1} (\mathbf{Q}_{\mathbf{u}}^t + \mathbf{Q}_{\mathbf{u}\mathbf{X}}^t \delta \mathbf{X}_t), \quad (30)$$

$$\begin{aligned} \mathbf{V}_{\mathbf{X}}^t &= \mathbf{Q}_{\mathbf{X}}^t - \mathbf{Q}_{\mathbf{u}\mathbf{X}}^{t\top} (\mathbf{Q}_{\mathbf{u}\mathbf{u}}^t)^{-1} \mathbf{Q}_{\mathbf{u}}^t = \mathbf{Q}_{\mathbf{X}}^t + \mathbf{Q}_{\mathbf{u}\mathbf{X}}^{t\top} \bar{\mathbf{k}}_t, \\ \mathbf{V}_{\mathbf{X}\mathbf{X}}^t &= \mathbf{Q}_{\mathbf{X}\mathbf{X}}^t - \mathbf{Q}_{\mathbf{u}\mathbf{X}}^{t\top} (\mathbf{Q}_{\mathbf{u}\mathbf{u}}^t)^{-1} \mathbf{Q}_{\mathbf{u}\mathbf{X}}^t = \mathbf{Q}_{\mathbf{X}\mathbf{X}}^t + \mathbf{Q}_{\mathbf{u}\mathbf{X}}^{t\top} \bar{\mathbf{K}}_t. \end{aligned} \quad (31)$$

To see whether the backward pass of the augmented value function inherits any implicit structure, let us rewrite Eq. (28) in a block-wise fashion by recalling Eq. (20).

$$\begin{aligned} \mathbf{Q}_{\mathbf{u}}^t &= \frac{1}{B} \sum_i \ell_{\mathbf{u}}^t |^{(i)} + \sum_i f_{\mathbf{u}}^t |^{(i)\top} [\mathbf{V}_{\mathbf{X}'}^t]_{B_{n_{t'}}^{(i)}} \\ [\mathbf{Q}_{\mathbf{X}}^t]_{B_{n_t}^{(i)}} &= \frac{1}{B} \ell_{\mathbf{x}}^t |^{(i)} + f_{\mathbf{x}}^t |^{(i)\top} [\mathbf{V}_{\mathbf{X}'}^t]_{B_{n_{t'}}^{(i)}} \\ [\mathbf{Q}_{\mathbf{u}\mathbf{X}}^t]_{(:,B_{n_t}^{(i)})} &= \frac{1}{B} \ell_{\mathbf{u}\mathbf{x}}^t |^{(i)} + \sum_j f_{\mathbf{u}}^t |^{(j)\top} [\mathbf{V}_{\mathbf{X}'\mathbf{X}'}^t]_{(B_{n_{t'}}^{(j)}, B_{n_{t'}}^{(i)})} f_{\mathbf{x}}^t |^{(i)} + [\mathbf{V}_{\mathbf{X}'}^t]_{B_{n_{t'}}^{(i)}} \cdot f_{\mathbf{u}\mathbf{x}}^t |^{(i)} \\ [\mathbf{Q}_{\mathbf{X}\mathbf{X}}^t]_{(B_{n_t}^{(i)}, B_{n_t}^{(j)})} &= \frac{1}{B} \delta_{ij} \ell_{\mathbf{x}\mathbf{x}}^t |^{(i)} + f_{\mathbf{x}}^t |^{(i)\top} [\mathbf{V}_{\mathbf{X}'\mathbf{X}'}^t]_{(B_{n_{t'}}^{(i)}, B_{n_{t'}}^{(j)})} f_{\mathbf{x}}^t |^{(j)} + \delta_{ij} ([\mathbf{V}_{\mathbf{X}'}^t]_{B_{n_{t'}}^{(i)}} \cdot f_{\mathbf{x}\mathbf{x}}^t |^{(j)}) \\ \mathbf{Q}_{\mathbf{u}\mathbf{u}}^t &= \frac{1}{B} \sum_i \ell_{\mathbf{u}\mathbf{u}}^t |^{(i)} + \sum_{ij} f_{\mathbf{u}}^t |^{(i)\top} [\mathbf{V}_{\mathbf{X}'\mathbf{X}'}^t]_{(B_{n_{t'}}^{(i)}, B_{n_{t'}}^{(j)})} f_{\mathbf{u}}^t |^{(j)} + \sum_i [\mathbf{V}_{\mathbf{X}'}^t]_{B_{n_{t'}}^{(i)}} \cdot f_{\mathbf{u}\mathbf{u}}^t |^{(i)} \end{aligned} \quad (32)$$

Notice that at $t = T$, the derivatives of the augmented value function are related to the ones for each sample by:

$$[\mathbf{V}_{\mathbf{X}}^T]_{B_{n_T}^{(i)}} = \frac{1}{B} V_{\mathbf{x}^{(i)}}^T, \text{ and } [\mathbf{V}_{\mathbf{X}\mathbf{X}}^T]_{(B_{n_T}^{(i)}, B_{n_T}^{(j)})} = \frac{1}{B} \delta_{ij} V_{\mathbf{x}^{(i)}\mathbf{x}^{(j)}}^T. \quad (33)$$

Substitute them into Eq. (32), one can show that the derivatives of the augmented \mathbf{Q} at $t = T - 1$ can indeed be expressed by the composition of each $Q^{(i)}$

$$\begin{aligned} \mathbf{Q}_u^{T-1} &= \frac{1}{B} \sum_i Q_u^{T-1}|^{(i)}, \quad [\mathbf{Q}_X^{T-1}]_{B_{n_t}^{(i)}} = \frac{1}{B} Q_{x^{(i)}}^{T-1}, \\ [\mathbf{Q}_{uX}^{T-1}]_{(:,B_{n_t}^{(i)})} &= \frac{1}{B} Q_{ux^{(i)}}^{T-1}, \quad [\mathbf{Q}_{XX}^{T-1}]_{(B_{n_t}^{(i)}, B_{n_t}^{(j)})} = \delta_{ij} \frac{1}{B} Q_{x^{(i)}x^{(j)}}^{T-1}, \quad \mathbf{Q}_{uu}^{T-1} = \frac{1}{B} \sum_i Q_{uu}^{T-1}|^{(i)}. \end{aligned} \quad (34)$$

However, \mathbf{V}_X^{T-1} and \mathbf{V}_{XX}^{T-1} will no longer preserve the structure described in Eq. (33). In fact, we will have

$$[\mathbf{V}_X^{T-1}]_{B_{n_{T-1}}^{(i)}} = \frac{1}{B} \left(Q_{x^{(i)}}^{T-1} - (Q_{ux^{(i)}}^{T-1})^\top (\mathbf{Q}_{uu}^{T-1})^{-1} \mathbf{Q}_u^{T-1} \right), \text{ and} \quad (35)$$

$$[\mathbf{V}_{XX}^{T-1}]_{(B_{n_{T-1}}^{(i)}, B_{n_{T-1}}^{(j)})} = \frac{1}{B} \left(\delta_{ij} Q_{x^{(i)}x^{(j)}}^{T-1} - (Q_{ux^{(i)}}^{T-1})^\top (\mathbf{Q}_{uu}^{T-1})^{-1} Q_{ux^{(j)}}^{T-1} \right). \quad (36)$$

Neither \mathbf{V}_X^{T-1} nor \mathbf{V}_{XX}^{T-1} can be expressed by the composition of $V_{x^{(i)}}^{T-1}$ or $V_{xx^{(i)}}^{T-1}$. Furthermore, \mathbf{V}_{XX}^{T-1} is no longer a block-diagonal matrix.

B.3 PseudoCode for the DDP Neural Optimizer

Algorithm 3 Batch Differential Dynamic Programming for Training Feedforward Networks (DDP Neural Optimizer)

Input: dataset \mathcal{D} , Tikhonov regularization δ_V, δ_Q , learning rate η , training iteration K , (optional) curvature factorization module $\text{CurvApprox}(\cdot)$

Initialize the nominal control trajectory $\bar{\mathbf{u}}^{(0)}$

for $k = 0$ **to** K **do**

 Sample batch initial state from dataset, $\{x_0^{(i)}\}_{i=1}^B \sim \mathcal{D}$

for $t = 0$ **to** $T - 1$ **do**

$$\mathbf{X}_{t+1} = \mathbf{F}_t(\mathbf{X}_t, \mathbf{u}_t^{(k)})$$

▷ Forward simulation

end for

 Set $\mathbf{V}_X^T = \nabla_X \Phi(\mathbf{X}_T)$ and $\mathbf{V}_{XX}^T = \nabla_{XX} \Phi(\mathbf{X}_T)$

for $t = T - 1$ **to** 0 **do**

 Compute $\mathbf{V}_H^t, \mathbf{V}_{HH}^t, \mathbf{Q}_X^t, \mathbf{Q}_u^t, \mathbf{Q}_{uX}^t, \mathbf{Q}_{XX}^t$ with Eq. (28-29)

▷ Backward pass

if $\text{CurvApprox}(\cdot)$ is available **then**

$$\bar{\mathbf{k}}_t \leftarrow \text{CurvApprox}(\mathbf{Q}_u^t; \{\mathbf{X}_t, \mathbf{V}_H^t\}_0^k)$$

$$\bar{\mathbf{K}}_t \leftarrow \text{CurvApprox}(\mathbf{Q}_{uX}^t; \{\mathbf{X}_t, \mathbf{V}_H^t\}_0^k)$$

else

 Compute \mathbf{Q}_{uu}^t with Eq. (28d) and set $\mathbf{Q}_{uu}^t \leftarrow \mathbf{Q}_{uu}^t + \delta_Q \mathbf{I}$

 Compute $\bar{\mathbf{k}}_t$ and $\bar{\mathbf{K}}_t$ by solving linear systems $\mathbf{Q}_{uu}^t \bar{\mathbf{k}}_t = -\mathbf{Q}_u^t$ and $\mathbf{Q}_{uu}^t \bar{\mathbf{K}}_t = -\mathbf{Q}_{uX}^t$

end if

 Compute $\mathbf{V}_X^t, \mathbf{V}_{XX}^t$ with Eq. (31) and set $\mathbf{V}_{XX}^t \leftarrow \mathbf{V}_{XX}^t + \delta_V \mathbf{I}$

end for

 Set $(\mathbf{X}_0^*, \bar{\mathbf{u}}^*) \leftarrow (\mathbf{X}_0, \bar{\mathbf{u}}^{(k)})$ and $(\text{loss}, \alpha) \leftarrow (\mathbf{J}(\bar{\mathbf{u}}^{(k)}; \mathbf{X}_0), 1)$

while $\mathbf{J}(\bar{\mathbf{u}}^*; \mathbf{X}_0) \geq \text{loss}$ and $\alpha \geq \alpha_{\min}$ **do**

for $t = 0$ **to** $T - 1$ **do**

$\mathbf{u}_t^* \leftarrow \mathbf{u}_t^{(k)} + \eta(\alpha \bar{\mathbf{k}}_t + \bar{\mathbf{K}}_t(\delta \mathbf{X}_t))$, where $\delta \mathbf{X}_t = \mathbf{X}_t^* - \mathbf{X}_t$. ▷ Additional forward pass

$$\mathbf{X}_{t+1}^* = \mathbf{F}_t(\mathbf{X}_t^*, \mathbf{u}_t^*)$$

end for

$\alpha \leftarrow \gamma \alpha$, where $\gamma < 1$ being the decay factor.

end while

$$\bar{\mathbf{u}}^{(k+1)} \leftarrow \bar{\mathbf{u}}^*$$

end for

C Others Derivations from the Main Text

C.1 Proof of Proposition 5

First observe the below lemma which connects the backward passes between two frameworks in the degenerate case.

Lemma 7. Assume $Q_{ux}^t = 0$ at all stages, then we have

$$V_x^t = H_x^t = p_t = J_{x_t}, \text{ and } V_{xx}^t = J_{x_t x_t}, \quad \forall t. \quad (37)$$

Proof. It is obvious to see that Eq. (37) holds at $t = T$. Now, assume the relation holds at $t + 1$ and observe that at the time t , the backward passes take the form of

$$\begin{aligned} p_t &= H_x^t = \ell_x^t + f_x^{t\top} p_{t+1} = J_{x_t}, \\ V_x^t &= Q_x^t - Q_{ux}^t (Q_{uu}^t)^{-1} Q_u^t = \ell_x^t + f_x^{t\top} V_x^{t+1}, \\ V_{xx}^t &= Q_{xx}^t - Q_{ux}^t (Q_{uu}^t)^{-1} Q_{ux}^t = \nabla_{x_t} \{ \ell_x^t + f_x^{t\top} V_x^{t+1} \} = J_{x_t x_t}, \end{aligned}$$

which concludes the proof. \square

Now, Eq. (13) follows by substituting Eq. (37) to the definition of Q_u^t and Q_{uu}^t

$$\begin{aligned} Q_u^t &= \ell_u^t + f_u^{t\top} V_x^{t+1} = \ell_u^t + f_u^{t\top} J_{x_{t+1}} = \nabla_{u_t} J, \\ Q_{uu}^t &= \ell_{uu}^t + f_u^{t\top} V_{xx}^{t+1} f_u^t + V_x^{t+1} \cdot f_{uu}^t \\ &= \ell_{uu}^t + f_u^{t\top} (\nabla_{x_{t+1}}^2 J) f_u^t + J_{x_{t+1}} \cdot f_{uu}^t \\ &= \nabla_{u_t} \{ \ell_u^t + f_u^{t\top} J_{x_{t+1}} \} = \nabla_{u_t u_t} J, \end{aligned}$$

where we denote $\nabla_{x_{t+1}}^2 \equiv \nabla_{x_{t+1} x_{t+1}}$ in the last two equations for simplicity. Consequently, the policy generates to layer-wise Newton update.

C.2 Derivation of Eq. (14)

Eq. (14) follows by a simple observation that the feedback term $\mathbf{K}_t \delta x_t \triangleq -(Q_{uu}^t)^{-1} Q_{ux}^t \delta x_t$ stands as the minimizer of the following objective

$$\mathbf{K}_t \delta x_t = \arg \min_{\delta u_t \in \Gamma'(\delta x_t)} \|\nabla_{u_t} Q(x_t + \delta x_t, u_t + \delta u_t) - \nabla_{u_t} Q(x_t, u_t)\|, \quad (38)$$

where $\Gamma'(\delta x_t)$ denotes all affine mappings from δx_t to δu_t and $\|\cdot\|$ can be any proper norm in the Euclidean space. Eq. (38) can be shown by Taylor expanding $Q(x_t + \delta x_t, u_t + \delta u_t)$ up to its first order,

$$\nabla_{u_t} Q(x_t + \delta x_t, u_t + \delta u_t) = \nabla_{u_t} Q(x_t, u_t) + Q_{ux}^t \delta x_t + Q_{uu}^t \delta u_t.$$

When $Q = J$, we will arrive at Eq. (14). While this is generally not true for nontrivial Q_{xu}^t (recall Proposition 5), we shall interpret the Bellman objective Q as the resulting objective when the feedback policies are applied to all the afterward stages, indeed implied in the Bellman equation Eq. (4).

D Experiment Detail

D.1 Setup

The networks in the classification problems are composed of 5-6 fully-connected layers. For the intermediate layers, we use ReLU activation on (F)MNIST, and Tanh on the other three data set. We use identity mapping at the last prediction layer for all data set except WINE, where we use sigmoid instead to help distinguish the performance among optimizers. The dimension of the hidden state is set to 10 for WINE, and 20-32 for other larger data set. The batch size is set to 8 for DIGITS, 16 for (F)MNIST, and 32 for WINE. Results reported in all plots and figures are averaged over multiple random seeds (3 seeds for (F)MNIST, and 6-10 for the rest). To accelerate training, we only utilize

50% of the samples in MNIST and FMNIST. Regarding the machine information, we conduct our experiments on GTX 1080 TI, RTX TITAN, and four Tesla V100 SXM2 16GB. For the baseline optimizers, we use the implementation in <https://github.com/Thrandis/EKFAC-pytorch> for KFAC and EKFAC.

D.2 Additional Experiment and Discussion

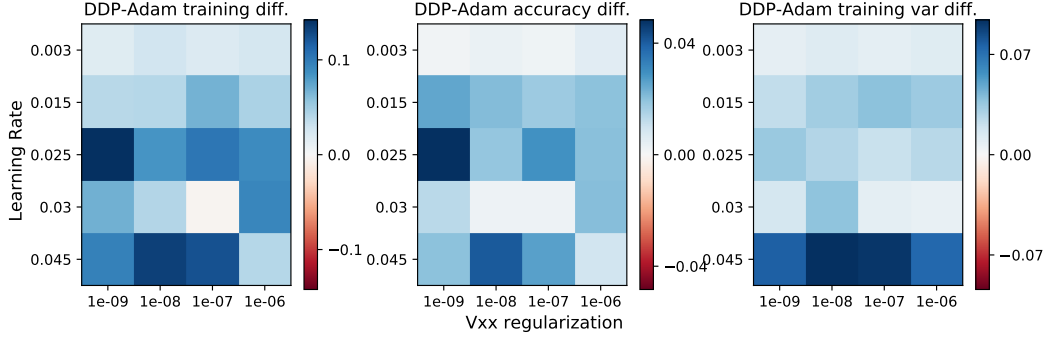


Figure 6: Additional experiment for Fig. 4a where we compare the performance difference between DDP-Adam vs Adam. All grids report values averaged over 10 random seeds. We use the same setup as in Fig. 4a.

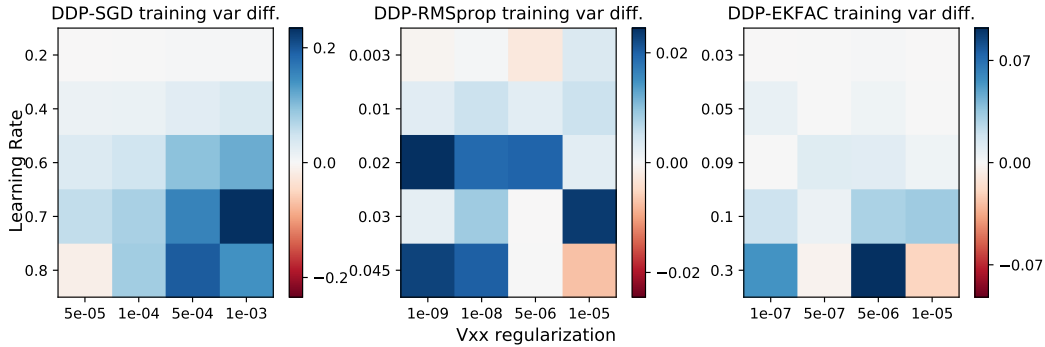


Figure 7: Performance difference on the variation of training over 10 random seeds, using the same setup as in Fig. 4a.

Effect on Variation Reduction during Training. Fig. 7 reports additional results on the variance difference during optimization. We use the same setup as in Fig. 4a, i.e. we keep all hyper-parameters the same for each experiment so that the performance difference only comes from the existence of feedback policies. For most cases, having additional updates from DDP stabilizes the training dynamics by reducing its variation over random initialization.

Hyper-parameter Tuning. Recall that in order to stabilize the training, we add Tikhonov regularization to both Q_{uu} and V_{xx} . In practice, we find that the regularization imposed on Q_{uu} generally has greater effect on the overall training dynamics. The performance can degrade when Q_{uu} is regulated either insufficiently or too much. On the other hands, effect of V_{xx} regularization on optimization is typically optimizer-dependent. Empirically, we find that regulating V_{xx} properly plays a key role in improving the performance of DDP-RMSprop, while the two rest are less sensitive to this hyper-parameter.

Computation Overhead. Lastly, Fig. 8 summarizes the computational overhead during DDP backward pass on DIGITS. Specifically, we compare the wall-clock processing time of DDP-EKFAC and DDP to the computation spent on the curvature approximate module in the DDP-EKFAC optimizer. The value thus suggests the additional overhead required for EKFAC to adopt the DDP framework, which includes second-order expansion on the value function, computing layer-wise feedback policies, etc. While the vanilla batch DDP scales poorly with the dimension of the hidden state under the current batch formulation, the overhead in DDP-EKFAC increases only by a *constant* (from 1.1 to 1.6) wrt different architecture setup, such as batch size, hidden dimension, and network

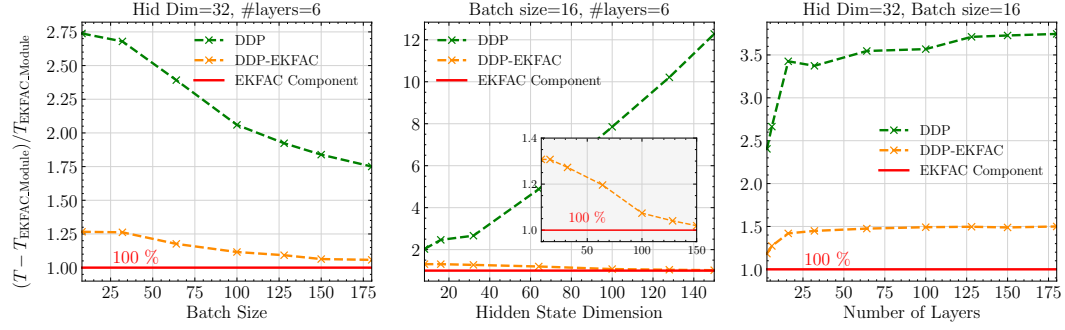


Figure 8: Overhead in the DDP backward pass compared with the computation spent on EKFAC curvature approximation (red line). We leave out the DDP curve in the middle inner plot to better visualize the overhead in DDP-EKFAC wrt hidden dimension.

depth. We stress that our current implementation is not fully optimized, so there is still room for further acceleration.